crystals

MDPI

Article

First-Principles Study of the Structural, Mechanical and Thermodynamic Properties of $Al_{11}RE_3$ in Aluminum Alloys

Touwen Fan [1,2], Lan Lin [1], Houjiang Liang [1], Yuhong Ma [1], Yuwei Tang [1], Te Hu [2,*], Zixiong Ruan [1], Dongchu Chen [2,*] and Yuanzhi Wu [1]

[1] School of Science and Research Institute of Automobile Parts Technology, Hunan Institute of Technology, Hengyang 421002, China
[2] School of Material Science and Hydrogen Energy Engineering, Foshan University, Foshan 528001, China
* Correspondence: wht5482@163.com (T.H.); chendc@fosu.edu.cn (D.C.)

Abstract: The stability and mechanical and thermodynamic properties of $Al_{11}RE_3$ intermetallics (RE = Sc, Y and lanthanide La-Lu) have been investigated by combining first-principles and Debye model calculations. It was found that the formation enthalpies of the $Al_{11}RE_3$ intermetallics are all negative, indicating that they are stable; moreover, the experimental values of $Al_{11}La_3$ and $Al_{11}Ce_3$ are in good agreement with the predicted values, which are −0.40 kJ/mol and −0.38 kJ/mol, respectively. The calculated results of the mechanical properties reveal that the Young's modulus E and shear modulus G of $Al_{11}RE_3$ (RE = La, Ce, Pr, Nd and Sm) intermetallics are obviously greater than that of Al, implying that the stiffness, toughness, and tensile strength of them are significantly greater than those of aluminum, and that they, as strengthen phases, can effectively improve the mechanical property of aluminum alloys. The Poisson's ratio v of $Al_{11}Sc_3$ (0.37) is the largest, and the heterogeneity is obvious. All the $Al_{11}RE_3$ intermetallics can enhance the thermostability of the aluminum because of their lower Gibbs free energy F in the range of −5.002~−4.137 eV/atom and thermal expansion coefficient α of Al in the range of 2.34~2.89 × 10^{-5}/K at 300K, as well as higher entropy and constant volume-specific heat than aluminum at finite temperatures. With an increase in the atomic number, different change trends were observed for the formation enthalpy ΔH_f, bulk modulus B, Young's modulus E, and shear modulus G. This paper can provide ideas and help for designing a high-performance, heat-resistant aluminum alloy.

Keywords: first-principles calculations; $Al_{11}RE_3$ phase; mechanical properties; quasi-harmonic approximation; elastic property

check for updates

Citation: Fan, T.; Lin, L.; Liang, H.; Ma, Y.; Tang, Y.; Hu, T.; Ruan, Z.; Chen, D.; Wu, Y. First-Principles Study of the Structural, Mechanical and Thermodynamic Properties of $Al_{11}RE_3$ in Aluminum Alloys. *Crystals* **2023**, *13*, 347. https://doi.org/10.3390/cryst13020347

Academic Editor: Sergio Brutti

Received: 17 January 2023
Revised: 8 February 2023
Accepted: 14 February 2023
Published: 17 February 2023

Copyright: © 2023 by the authors. Licensee MDPI, Basel, Switzerland. This article is an open access article distributed under the terms and conditions of the Creative Commons Attribution (CC BY) license (https://creativecommons.org/licenses/by/4.0/).

1. Introduction

Aluminum (Al) alloys have become an important lightweight material for energy conservation and emission reduction in the automobile, rail transit, aerospace, and other industries due to their many excellent performances, including their light weight, high specific strength, good formability, excellent weldability, and corrosion resistance [1–6]. As engineering materials, Al alloys have been widely used at room temperature; however, it is difficult to meet the requirements of high-temperature devices, such as aircraft and automobile engines, that have been used for a long time at more than 200 °C [7,8]. The cause of this issue is the rapid coarsening and dissolution of the strengthen phases in the Al alloys at high temperature, which leads to a sharp decrease in the mechanical properties of the alloys [9,10]. Therefore, improving the thermal stability of the strengthen phases at high temperatures is the key to expanding the application of Al alloys in high-temperature devices.

In recent years, alloying by adding rare-earth elements (RE) has become an important and effective method to improve the high-temperature performance of the Al alloys, mainly because of the formation of the high temperature-resistant strengthen phases and Al_xRE_y

intermetallics in the alloy, such as the $L1_2$-Al_3RE (e.g., RE = Sc, Er) [11–14] and $Al_{11}RE_3$ (e.g., RE = La, Ce) intermetallics [15–18]. It is widely known that the physical and mechanical properties of alloys mainly depend on the basic properties of the strengthen phases. Consequently, the research hotspots about $Al_{11}RE_3$ alloys focus on the basic properties of the Al_xRE_y intermetallics, and the relevant research results have been obtained through experimentation.

Nevertheless, through experimentation, an investigation of all the Al_xRE_y intermetallics would require the synthesis, processing, and characterization of many $Al_{11}RE_3$ alloys, making it complex, inefficient, and very expensive. Instead, the theoretical identification, e.g., first-principles calculations, which plays a very important role in materials research, particularly in complicated systems, can make this work easier and cheaper because of the development of modern computer technology [19–22].

In fact, there have been systematic studies on the basic properties of first-principles calculations, including on the stability, elastic parameters, and thermal properties, such as free energy, entropy, constant volume heat capacity, and the volume thermal expansion of the $L1_2$-Al_3RE strengthen phases in Al alloys [23–25]. However, to our best knowledge, no systematic first-principles computational studies have been performed on $Al_{11}RE_3$ intermetallics. In this work, we have used the first-principles calculations combined with quasi-harmonic approximation to investigate the structural, elastic, thermal, and electrical properties of the $Al_{11}RE_3$ (Sc, Y, and lanthanide La-Lu) intermetallics in Al-based alloys at various temperatures and pressures. The lattice constant, lattice mismatch, and formation enthalpy of $Al_{11}RE_3$ compounds are firstly calculated, and the underlying mechanisms are probed. Then, the thermodynamic parameters of $Al_{11}RE_3$ compound are calculated using a Debye model to understand the high temperature performance of aluminum alloys.

2. Computation Detail

First-principles calculations based on density functional theory (DFT) [26] employed the plane-wave, total-energy methodology, which solved the Kohn–Sham equation to obtain the valence electron density and the wave function as implemented in the Vienna ab initio Simulation Package (VASP) [27]. The interaction between the ionic core and valence electrons [28] was described by the Projector Augmented Wave (PAW) [29] method, and the exchange correlation function was calculated using the Perdew–Burke–Ernzerhof (PBE) version of the generalized gradient approximation (GGA) [30]. To ensure that the results are accurate, the cutoff energy of the plane-wave basis was chosen as 350 eV, and Brillouin zone sampling was performed using the Gamma-centered Monkhorst–Pack method with $8 \times 3 \times 3$ k–mesh grids [31]. To obtain a better calculation and accurate results, the ground state geometry was relaxed using conjugate gradient (CG) minimization, and the cell shape and internal atomic coordinates were completely relaxed until the electron self-consistent convergence criterion of the electron iteration was 10^{-6} eV/atom and the Hellmann–Feynman force [32] was less than 0.01 eV/Å. In the calculation process, the PAW_GGA pseudopotentials of Al, Sc, La, Y_sv, and (Ce-Lu)_3 are used to simulate the size of the real potential. The energy–strain method was used for the mechanical calculation, the VASPKIT code [33] was used to fit the equation of state (EOS), and the strain values were −9% ~9%. The thermodynamic properties were calculated by establishing the Debye–Grüneisen model [34,35] and using the Gibbs2 code [36]. Although it is possible to calculate the thermodynamic properties of the material using the quasi harmonic approximation model (QHA), it is still a complex and expensive task to calculate the full vibration spectrum of the crystal on the volume grid. At the same time, compared with a fixed Poisson's ratio v in Debye–Grüneisen model, the exact Poisson's ratio v of each alloy is calculated using energy strain method in this experiment, which further improves the accuracy on the basis of the original. However, the Debye model only considers the contribution of the long wave part but not the short wave part, which makes the error of calculation at a high temperature larger. At the same time, the $Al_{11}RE_3$ unit cell model required for the calculation was derived by the program software of VESTA to visualize the 3D structure,

as shown in Figure 1a. It can be seen from the following figure that the structure belongs to the orthorhombic crystal system.

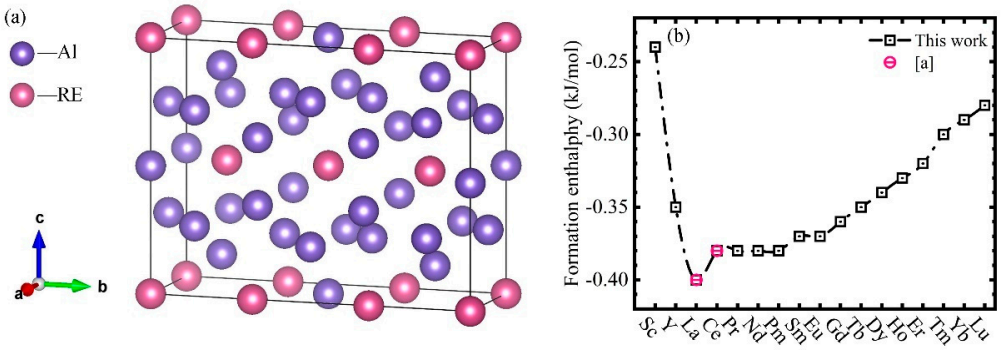


Figure 1. (**a**) The unit cell model of $Al_{11}RE_3$; (**b**) the comparison between the calculated and experimental values of the formation enthalpy of $Al_{11}RE_3$. Ref. [a] represents [20].

3. Result and Discussion

3.1. Enthalpy of Formation and Stability

For the purpose of evaluating the relative stabilities of the $Al_{11}RE_3$ intermetallics in Al alloys, we calculated the formation enthalpy ΔH_f according to the following equation [37]

$$\Delta H_f = \frac{E_{tot} - xE_{Al} - yE_{RE}}{x + y} \quad (1)$$

where E_{tot} is the total energy of different compounds; E_{Al} and E_{RE} are the calculated total energy of the elements of Al and RE in a steady state, respectively. Parameters x and y are the number of Al and RE atoms in the unit cell, respectively.

Based on the calculated formation enthalpy ΔH_f of $Al_{11}RE_3$ intermetallics and the previous theoretical data [20] at 0 K and 0 GPa, as shown in Figure 1b, we can obtain the following conclusions: (1) The calculated values were in good agreement with the previous theoretical predictions, which indicates that the present calculations are accurate and reliable; (2) the formation enthalpies of the $Al_{11}RE_3$ intermetallics are all negative, indicating that they are stable compounds; (3) with an increase in the atomic number, the formation enthalpy decreases first and then increases. The maximum and minimum values of the ΔH_f appear at the Sc and La elements, respectively, which indicates that the thermodynamic stability of $Al_{11}La_3$ is the strongest, followed by $Al_{11}Ce_3$, while the thermodynamic stability of $Al_{11}Sc_3$ is the worst. These results are in good agreement with the experimental findings that $Al_{11}La_3$ and $Al_{11}Ce_3$ particles are the most found compounds in the experiment [38].

In this experiment, the formation enthalpy ΔH_f of the aluminum alloy $Al_{11}RE_3$ doped with 11 rare earth elements was calculated according to the formula. Compared with the existing experimental values [20], as shown in Figure 2, it can be clearly seen that the existing experimental values of $Al_{11}La_3$ and $Al_{11}Ce_3$ are in good agreement with the existing theoretical predicted values, which are -0.40 kJ/mol and -0.38 kJ/mol, respectively. We can observe that the formation enthalpies of the binary aluminum alloys are all negative, indicating that there are exothermic reactions when they form compounds, and that they are all stable compounds [20]. At the same time, Figure 1b also helps us better understand the relationship between the formation enthalpy ΔH_f and the atomic number of rare earth elements. We can clearly observe that the overall curve shows a trend that first decreases and then increases. Moreover, the formation enthalpy ΔH_f reaches the maximum value at the Sc element and then shows a downward trend; the lanthanide rare earth element La reaches a minimum value of -0.40 eV/atom, and the atomic number increases until the Lu element shows a generally upward trend; however, the formation enthalpy ΔH_f of the

Sc element is not exceeded. This shows that the thermodynamic stability of $Al_{11}La_3$ is the strongest [38], while the thermodynamic stability of $Al_{11}Sc_3$ is the weakest.

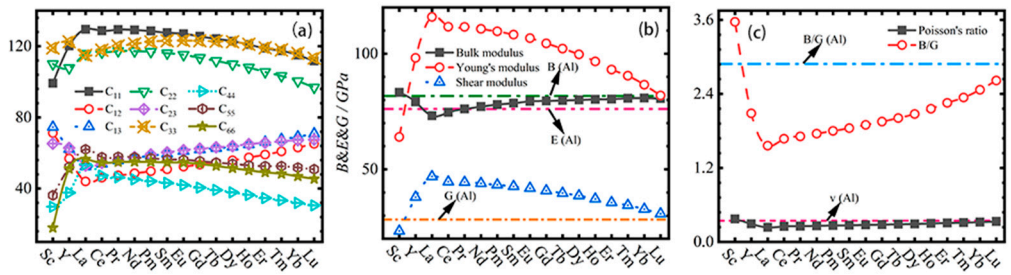


Figure 2. (**a**) Calculated elastic constant of $Al_{11}RE_3$; (**b**) Young's modulus E, shear modulus G, bulk modulus B values; (**c**) Poisson's ratio ν and B/G values.

3.2. Elastic Properties

Elastic constants and elastic moduli are important components in understanding the mechanical properties of materials [39]. The elastic constant can be used to determine the mechanical stability of the material, reflect the ability of the crystal to resist external stress [20], and obtain important information on the stability of the aluminum alloy unit cell structure and the anisotropic characteristics of the crystal. By calculating the elastic constant of the alloy [40], the elastic modulus such as bulk modulus B, shear modulus G, Young's modulus E, and Poisson's ratio ν can be further determined to determine the mechanical properties of the material. The elastic constant is first calculated from a small strain of a uniform unit cell and is then determined by using the corresponding change in the total energy [41]; finally, the elastic modulus is derived using the Voigt–Reuss–Hill approximation [42].

C_{ij} is the crystal's response to an applied external stress, while the number of elastic constants lies in the symmetry of the structure. $Al_{11}RE_3$ is an orthorhombic structure with nine independent elastic constants ($C_{11}, C_{12}, C_{13}, C_{22}, C_{23}, C_{33}, C_{44}, C_{55}$, *and* C_{66}), whose elastic constant matrix is in the form of 6×6. On the basis of the Born criterion [43], according to the necessary and sufficient Born criterion under the simplified orthogonal system [44], the following criteria can be obtained:

$$C_{11} > 0, \quad C_{11}C_{22} > C_{12}^2 \tag{2}$$

$$C_{11}C_{22}C_{33} + 2C_{12}C_{13}C_{22} - C_{11}C_{23}^2 - C_{22}C_{13}^2 - C_{33}C_{12}^2 > 0 \tag{3}$$

$$C_{44} > 0\,, \quad C_{55} > 0\,, \quad C_{66} > 0 \tag{4}$$

Table 1 and Figure 2 present the relevant elastic constants and elastic moduli, respectively, which are used to determine the mechanical stability of aluminum alloys and the mechanical properties of materials.

Hill proved that the equations obtained using the Voigt–Reuss description of the bulk modulus B and the shear modulus G are the upper and lower limits of the true crystal constant, respectively, which is exactly the arithmetic mean provided by Voigt and Reuss; moreover, the following obtains the orthorhombic crystal formulas for calculating the elastic modulus and shear modulus [42]

$$B = \frac{B_R + B_V}{2} \tag{5}$$

$$G = \frac{G_R + G_V}{2} \tag{6}$$

$$B_R = \frac{N^2}{M} \tag{7}$$

Table 1. The elastic constant C_{ij} of $Al_{11}RE_3$ intermetallics (units: GPa).

Compound	C_{11}	C_{12}	C_{13}	C_{22}	C_{23}	C_{33}	C_{44}	C_{55}	C_{66}
$Al_{11}Sc_3$	99.22	71.22	74.54	110.05	65.24	119.06	29.81	36.21	17.95
$Al_{11}Y_3$	120.17	56.87	62.15	107.78	62.81	122.48	37.68	52.18	51.12
$Al_{11}La_3$	129.53	44.00	52.36	115.74	52.97	114.94	53.59	62.02	56.55
$Al_{11}Ce_3$	128.71	46.13	53.92	116.61	54.39	117.82	47.36	57.64	54.54
$Al_{11}Pr_3$	129.35	47.41	55.74	117.31	56.11	120.19	46.33	57.83	54.93
$Al_{11}Nd_3$	129.12	48.55	57.23	117.25	57.67	121.31	45.19	57.52	55.06
$Al_{11}Pm_3$	128.51	49.71	58.47	116.87	59.17	122.52	44.13	57.03	55.03
$Al_{11}Sm_3$	127.56	50.86	59.50	116.08	60.35	123.12	43.20	56.36	54.69
$Al_{11}Eu_3$	127.00	52.31	61.07	115.20	61.62	123.22	42.01	56.17	54.60
$Al_{11}Gd_3$	125.51	53.43	61.95	113.46	62.39	123.07	40.54	55.41	53.81
$Al_{11}Tb_3$	124.19	54.61	62.72	111.77	63.18	122.77	39.24	54.61	52.76
$Al_{11}Dy_3$	122.83	55.88	63.48	109.92	63.90	122.49	37.87	53.88	51.47
$Al_{11}Ho_3$	120.95	57.45	64.74	108.04	64.96	121.11	36.43	53.09	50.23
$Al_{11}Er_3$	118.82	59.06	66.18	105.53	65.82	119.16	34.70	52.59	49.13
$Al_{11}Tm_3$	117.47	60.86	67.65	103.33	66.59	117.93	33.43	52.59	48.32
$Al_{11}Yb_3$	115.03	63.04	69.11	100.37	67.20	116.02	31.97	51.82	46.91
$Al_{11}Lu_3$	111.69	65.12	70.84	96.90	67.55	113.29	30.53	50.89	45.44

$$B_V = \frac{2(C_{11} + C_{12}) + C_{33} + 4C_{13}}{9} \tag{8}$$

$$G_R = \frac{15}{18(B_v/N^2) + [6/(C_{11} - C_{12})] + (6/C_{44}) + (3/C_{66})} \tag{9}$$

$$G_v = \frac{M + 3C_{11} - 3C_{12} + 12C_{44} + C_{66}}{30} \tag{10}$$

where

$$M = C_{11} + C_{12} + 2C_{33} - 4C_{13} \tag{11}$$

$$N^2 = (C_{11} + C_{12})C_{33} - 2C_{13}^2 \tag{12}$$

Using the elastic constants, Young's modulus E and Poisson's ratio ν can be expressed as:

$$E = \frac{9GB}{3B + G} \tag{13}$$

$$v = \frac{3B - 2G}{2(3B + G)} \tag{14}$$

According to the criterion of mechanical stability and the calculated value of the elastic constant, we can observe from Figure 2a that their values are positive, and that all the rare earth–aluminum alloys meet the conditions of mechanical stability, indicating that they are stable. We can also see from Figure 2a that there are two trends in relation to the La element, as the node shows a trend of first increasing and then decreasing, or first decreasing and then increasing.

Bulk modulus B can be used to measure the average atomic bond strength of a material and is inversely proportional to compressibility; the greater the bulk modulus, the greater the resistance of the material to compression [45]. Observing the bulk modulus B of $Al_{11}RE_3$ and aluminum in Figure 2b, it is found that the bulk modulus of all aluminum rare earth alloys except $Al_{11}Sc3$ (83.21 GPa) is smaller than that of Al (81.71 GPa), of which $Al_{11}La_3$ has the smallest bulk modulus B, and that the minimum is 73.15 GPa. This shows that $Al_{11}Sc_3$ has the strongest compressive ability, the most stable structure, is not easily deformed, has the strongest rigidity and the highest hardness. On the contrary, $Al_{11}La_3$ is easy to deform, weak in rigidity, and is the lowest in hardness.

Young's modulus E and shear modulus G are the most important parameters for evaluating the strength of materials. Young's modulus E can represent the ability to resist

deformation; the larger the value, the harder the material. In addition, the shear modulus G can represent the ability to resist shear stress, and the larger the shear modulus, the more obvious the directional bonds between atoms [45]. It can be seen from Figure 2b that the shear modulus G and Young's modulus E of $Al_{11}RE_3$ have the same trend, with La atoms as the nodes, of first rising and then decreasing with an increase in the atomic number. With $Al_{11}Sc_3$ as the starting point, Young's modulus E increases from 64.00 GPa to 115.81 GPa for $Al_{11}La_3$ and then slowly decreases to $Al_{11}Lu_3$ (81.91 GPa) with an increase in the atomic number. Similarly, the shear modulus G also showed the same trend, rising from 23.33 GPa at $Al_{11}Sc_3$ to 46.88 GPa at $Al_{11}La_3$ and then slowly decreasing to 30.78 GPa. The Young's modulus E and shear modulus G of aluminum are 76.11 GPa and 28.30 GPa, respectively. It is obvious that the addition of RE elements makes the Young's modulus E and shear modulus G of the aluminum alloy higher than that of aluminum, except for Sc. Among them, $Al_{11}La_3$ has the highest Young's modulus E value and shear modulus G value, which are greatly improved compared with aluminum, which are increased by about 52% and 66%, respectively. After adding rare earth elements (except Sc), the stiffness of the aluminum alloy material increases, the toughness is good, the material is not easily deformed, and the tensile strength is significantly improved. In contrast, the shear modulus G of $Al_{11}Sc_3$ is about 18% lower than that of aluminum, and the Young's modulus E is about 16% lower than that of aluminum, indicating that the element Sc does not enhance its elastic properties, and that the formed aluminum-based alloy is volatile. Moreover, stiffness and strength decrease, and elastic deformation increases.

Poisson's ratio ν can be used to predict the plasticity of the material, thereby quantifying the stability of the crystal against shearing [20,46]. It also represents the ratio of the lateral strain to the longitudinal strain of the solid medium; therefore, the range of Poisson's ratio is greater than 0, the Poisson's ratio is in the range of 0.1~0.3, and the material is hard; when Poisson's ratio is 0.4~0.5, the material is generally fluid or soft. Figure 2c shows that $Al_{11}La_3$ has the lowest Poisson's ratio of 0.24, which is also in the range of 0.1 to 0.3, which belongs to an alloy with high hardness. Generally speaking, aluminum has low hardness, high plasticity, and is easy to process. It can be seen from Figure 2c that the Poisson's ratios of Al, $Al_{11}Sc_3$, and $Al_{11}Er_3$~$Al_{11}Lu_3$ are all between 0.3 and 0.4, with certain plasticity and low hardness. At the same time, Poisson's ratio v can reflect the heterogeneity of materials. Taking the Poisson's ratio v = 0.26 as the boundary, except for $Al_{11}Ce_3$ and $Al_{11}La_3$, all aluminum-based alloys exhibit uneven deformation, and the Poisson's ratio v of $Al_{11}Sc_3$ (0.37) is the largest, and the heterogeneity is obvious.

B/G can also be used to characterize the plasticity of the material: with a *B/G* of 1.75 as the boundary [47], below 1.75, the material is ductile, and, above 1.75, the material is brittle [20,45]. As shown in Figure 2c, the Poisson's ratio v and *B/G* of the aluminum alloy both decrease first and then increase with an increase in the rare earth atomic number, taking the La element as the node. Among them, the B/G of $Al_{11}La_3$, $Al_{11}Ce_3$, and $Al_{11}Pr_3$ are all lower than 1.75, with values of 1.56, 1.67, and 1.71, respectively, showing certain ductility. The value of $Al_{11}La_3$ is the smallest, which indicates that the ductility is good and that the rolling degree is improved, which is beneficial to the production of precision materials. The *B/G* value of $Al_{11}Sc_3$ is up to 3.567, which is not conducive to rolling.

3.3. The Thermodynamic Properties

In order to understand the thermodynamic properties of the second-phase particles of the material, this calculation uses the Debye theory (DT) [35] to obtain a model of crystal vibration [48–50], namely, the Debye–Grüneisen model, and the key is to calculate the Debye function Θ_D(V) through the Debye cutoff frequency ω_D [51–53]. At high temperature [54–56], the $Al_{11}RE_3$ phase will be decomposed into Al and Al_2RE; in this work, we adopt P = 0 at a temperature of 0–1000 K [57] for the thermodynamic calculation of the aluminum alloy, according to the following equation [51–53]:

$$\frac{h}{2\pi}\omega_D = \kappa_B\Theta_D \tag{15}$$

where the h and κ_B are Plank's and Boltzmann's constants, respectively. The ω_D can be obtained using the Debye sound velocity v_D:

$$\omega_D = \left(\frac{6\pi^2}{V}\right)^{1/3} v_D \tag{16}$$

where the V is the volume of the solid. There are three different types of sound velocity in solids, all of which are anisotropic. For isotropic media, Anderson expresses the low temperature average for the sound velocity for an isotropic crystal as:

$$\frac{1}{v_D^3} = \frac{1}{3}\left(\frac{1}{v_L^3} + \frac{2}{v_S^3}\right) \tag{17}$$

where v_L and v_S are longitudinal and transverse sound velocities and can be expressed as $v_L = \sqrt{(L/\rho)}$ and $v_S = \sqrt{(S/\rho)}$, respectively. With Equations (14)–(17), a simpler method can be obtained to calculate v_D and Θ_D; then, they are used to calculate the longitudinal and transverse moduli as follows:

$$L = \frac{3(1-v)}{1+v}B, \qquad S = \frac{3(1-2v)}{2(1+v)}B \tag{18}$$

Then, the v_D can be obtained:

$$v_D = f(v)\sqrt{\frac{B}{\rho}} \tag{19}$$

$$f(v) = \left\{\frac{1}{3}\left[\left[\frac{1+v}{3(1-v)}\right]^{3/2} + 2\left[\frac{2(1+v)}{3(1-2v)}\right]^{3/2}\right]\right\}^{-1/3} \tag{20}$$

It has been proved that the method can obtain reasonable Debye sound velocity. Therefore, the Θ_D can be calculated from the bulk modulus and density using the following equation:

$$\Theta_D = f(v)\frac{h}{2\pi\kappa_B}\left(48\pi^5\right)^{1/6}\sqrt{\frac{r_0 B}{M}} \tag{21}$$

where M is the atomic weight and $r0$ is the equilibrium Wigner–Seitz radius.

After inserting the Θ_D into quasi harmonic formula, the Helmholtz free energy F, entropy S, heat capacity CV, and thermal expansion α can be, respectively, described by [34,53]:

$$F(V,T) = E(V) - \kappa_B T\left\{D\left(\frac{\Theta_D}{T}\right) - 3\ln\left[1 - e^{\left(\frac{-\Theta_D}{T}\right)}\right] + \frac{9}{8}\kappa_B\Theta_D\right\} \tag{22}$$

$$C_V = 3\kappa_B\left[4D(\Theta_D/T) - \frac{3\Theta_D/T}{exp(\Theta_D/T) - 1}\right] \tag{23}$$

$$S = 3\kappa_B\left\{\frac{4}{3}D(\Theta_D/T) - \ln[1 - exp(-\Theta_D/T)]\right\} \tag{24}$$

$$\gamma_D = -\frac{ln\partial\Theta_D}{ln\partial lnV}, \qquad \alpha = \frac{\gamma C_V}{B_0 V} \tag{25}$$

At a temperature of 0–1000 K, the Gibbs free energy F, entropy S, thermal melt C_V, and thermal expansion coefficient α are shown in Figure 3a–d.

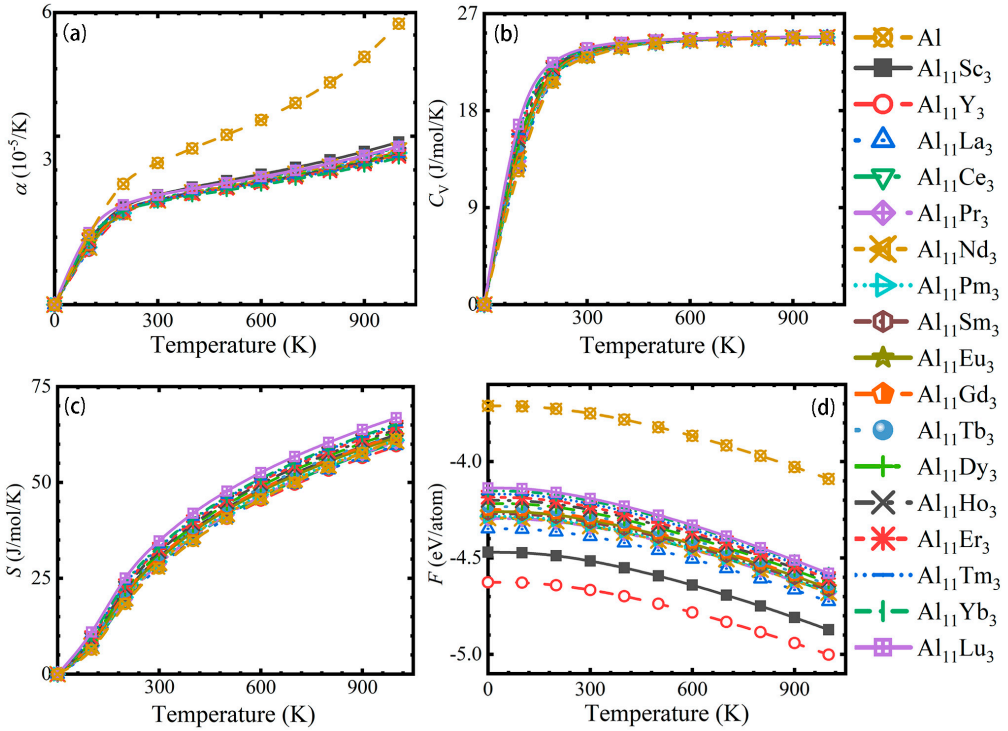


Figure 3. Aluminum and $Al_{11}RE_3$ at T = 0–1000 K, (**a**) thermal expansion coefficient α as a function of temperature T; (**b**) constant volume specific heat C_V; (**c**) entropy S; (**d**) Gibbs free energy F.

As shown in Figure 3a–c, it is found that the thermal expansion coefficient α, constant volume specific heat C_V, and entropy S of the aluminum and rare earth aluminum alloys all increase with an increase in temperature of ~1000 K; however, the increase range is different.

The thermal expansion coefficient α can be used to characterize the ability of an object to expand and contract due to temperature changes. In Figure 3a, the initial and final values of thermal expansion coefficients and growth rates of 17 $Al_{11}RE_3$ alloys are basically the same, i.e., in the order of ~2.89 × 10^{-5}/K. In detail, at 0–200 K, there is a relatively large increase, and, after 200 K, the growth rate is slow. The change of thermal expansion coefficient α of an Al of ~5.00 × 10^{-5}/K with T is significantly larger than that of $Al_{11}RE_3$, indicating that the thermal stability of the aluminum element is poor, and that the addition of rare earth elements greatly improves the thermal stability of the aluminum element. Aluminum alloy can maintain a good stable state even at high temperature, suitable for high temperature resistant aluminum alloy materials.

As shown in Figure 3b, the constant volume specific heat C_V of Al and $Al_{11}RE_3$ both showed a significant increase, then a slow increase, and, finally, a gradual increase. The constant volume specific heat C_V of RE aluminum alloys grows the most at 0–200 K, increasing exponentially, and then the growth rate slows down significantly at 200–600 K, and basically stabilizes after 600 K. The specific heat C_V value $Al_{11}RE_3$ of ~24.86 J/mol/K and the growth rate are both higher than those of the Al of ~24.81 J/mol/K. The growth rates of rare earth aluminum alloys are basically the same, and the constant volume specific heat C_V of $Al_{11}RE_3$ tends to be consistent. Since the constant volume specific heat C_V of an RE aluminum alloy is greater than that of aluminum, it means that, at a certain temperature, the heat absorption or heat dissipation ability of an aluminum alloy after adding RE elements is stronger than that of aluminum.

The entropy S value indicates that the system changes from an ordered state to a disordered state. The entropy S value increases with temperature because molecular motion becomes more violent with an increasing temperature and will deviate more from its equilibrium position. Looking at Figure 3c, the entropy S curves of aluminum of

~61.27 J/mol/K and aluminum alloys of ~66.86 J/mol/K have been increasing with an increase in temperature; moreover, although the growth rate has decreased, the growth rate and growth value are higher than those of aluminum. The entropy growth and growth trend among the 17 kinds of aluminum alloys are very close, indicating that the addition of RE elements does not mean that the aluminum alloys are greatly affected by temperature and have good consistency.

As shown in Figure 3d, it is found that the Gibbs free energies *F* of both aluminum and $Al_{11}RE_3$ alloys are less than 0, which have an Al value of ~−3.712 eV/atom and $Al_{11}RE_3$ alloys of ~4.137 eV/atom, indicating that they exist stably. At 0 and 1000 K, the Gibbs free energies of lanthanides are also very close, while the initial and final values of Sc and Y are smaller than those of lanthanides. It is also clearly observed that the variation curves of the Gibbs free energy *F* of the aluminum alloy with the temperature *T* all decrease, and that the decreasing range is consistent. At the same time, the Gibbs free energy of 17 RE aluminum alloys is lower than that of aluminum, which means that the addition of rare earth elements improves the stability of aluminum.

The variation of the thermal expansion coefficient a of the aluminum element with the temperature *T* is significantly larger than that of $Al_{11}RE_3$, indicating that the thermal stability of the aluminum is poor, and that the addition of rare earth elements greatly improves the thermal stability of the aluminum alloy, making the aluminum alloy exist even at high temperatures. Nevertheless, it can still maintain good stability in the state and is suitable for high temperature-resistant aluminum alloy materials.

4. Conclusions

In summary, the stability, mechanical properties, and thermodynamic properties of eleven $Al_{11}RE_3$ intermetallics at 0–1000 K were investigated by combining the first-principles calculations and the Debye model. The results of the study are as follows:

(1) The enthalpy of formation ΔH_f of $Al_{11}RE_3$ intermetallics are all negative values, all belong to exothermic reactions, and are all stable compounds. The thermodynamic stability of $Al_{11}La_3$ is the strongest, while the thermodynamic stability of $Al_{11}Sc_3$ is the weakest;

(2) Comparing the mechanical constants of the eleven $Al_{11}RE_3$ intermetallics, it is found that the stiffness, toughness, and tensile strength of the $Al_{11}RE_3$ intermetallics (RE = La, Ce, Pr, Nd, Sm) are significantly greater than those of aluminum, which indicates that these $Al_{11}RE_3$ intermetallics act as strengthen phases that can effectively improve the mechanical property of aluminum;

(3) The Debye–Grüneisen model was used to analyze the thermodynamic properties (Gibbs free energy, constant volume specific heat, entropy, and thermal expansion coefficient) of the eleven $Al_{11}RE_3$ intermetallics at a range of 0–1000 K, and the results consistently showed that the $Al_{11}RE_3$ intermetallics act as strengthen phases that can improve the thermal stability of the aluminum. In the process of temperature change, $Al_{11}Pm_3$ and $Al_{11}Sm_3$ are most affected by temperature and easily become unstable; their heat absorption and heat dissipation capabilities are also stronger than other RE aluminum alloys;

(4) With an increase in the atomic number, different change trends were observed for the formation enthalpy ΔH_f, bulk modulus *B*, Young's modulus *E*, and shear modulus *G*, which decreases first.

Author Contributions: Methodology, T.F. and H.L.; validation, Y.W.; investigation, T.F. and L.L.; resources, H.L., Y.M., Y.T., Z.R., D.C. and Y.W.; data curation, H.L., Y.M., Y.T., Z.R., D.C. and Y.W.; writing—original draft, L.L.; writing—review & editing, T.F., T.H. and Z.R.; visualization, L.L.; Pproject administration, H.L., Y.M., Y.T., D.C. and Y.W. All authors have read and agreed to the published version of the manuscript.

Funding: This work was supported by the R & D plan for key areas in Guangdong Province (2020B010186001, 2020B1515120093), R & D plan for key areas in Jiangxi Province (20201BBE51009), the Scientific Research Project of Hunan Institute of Technology (HQ21016, 21A0564, HP21047, 2022CE024), the Natural Science Foundation of China (52171115). and the APC was funded by [HQ21016, 21A0564, HP21047, 2022CE024].

Data Availability Statement: The data presented in this study are openly available in Crystals at https://doi.org/10.3390/cryst13020347.

Acknowledgments: This work is supported by the R & D plan for key areas in Guangdong Province (2020B010186001, 2020B1515120093), R & D plan for key areas in Jiangxi Province (20201BBE51009), the Scientific Research Project of Hunan Institute of Technology (HQ21016, 21A0564, HP21047, 2022CE024), the Natural Science Foundation of China (52171115).

Conflicts of Interest: The authors declare that they have no known competing financial interest or personal relationship that could have appeared to influence the work reported in this paper.

References

1. Azarniya, A.; Hosseini, H.R.M. A new method for fabrication of in situ Al/Al_3Ti–Al_2O_3 nanocomposites based on thermal decomposition of nanostructured tialite. *J. Alloys Compd.* **2015**, *643*, 64–73. [CrossRef]
2. Azarniya, A.; Taheri, A.K.; Taheri, K.K. Recent advances in ageing of 7xxx series aluminum alloys: A physical metallurgy perspective. *J. Alloys Compd.* **2019**, *781*, 945–983. [CrossRef]
3. Canakci, A.; Varol, T. Microstructure and properties of AA7075/Al–SiC composites fabricated using powder metallurgy and hot pressing. *Powder Technol.* **2014**, *268*, 72–79. [CrossRef]
4. Patel, V.K.; Bhowmik, S. Plasma processing of aluminum alloys to promote adhesion: A critical review. *Rev. Adhes. Adhes.* **2017**, *5*, 79–104. [CrossRef]
5. Singh, J.; Chauhan, A. Characterization of hybrid aluminum matrix composites for advanced applications—A review. *J. Mater. Res. Technol.* **2016**, *5*, 159–169. [CrossRef]
6. Seidman, D.N.; Marquis, E.A.; Dunand, D.C. Precipitation strengthening at ambient and elevated temperatures of heat-treatable Al(Sc) alloys. *Acta Mater.* **2002**, *50*, 4021–4035. [CrossRef]
7. Farkoosh, A.R.; Pekguleryuz, M. The effects of manganese on the T-phase and creep resistance in Al–Si–Cu–Mg–Ni alloys. *Mater. Sci. Eng. A* **2013**, *582*, 248–256. [CrossRef]
8. Qian, F.; Jin, S.; Sha, G.; Li, Y. Enhanced dispersoid precipitation and dispersion strengthening in an Al alloy by microalloying with Cd. *Acta Mater.* **2018**, *157*, 114–125. [CrossRef]
9. Jin, L.; Liu, K.; Chen, X.G. Evolution of dispersoids and their effects on elevated-temperature strength and creep resistance in Al-Si-Cu 319 cast alloys with Mn and Mo additions. *Mater. Sci. Eng. A* **2020**, *770*, 138554. [CrossRef]
10. Farkoosh, A.R.; Chen, X.G.; Pekguleryuz, M. Dispersoid strengthening of a high temperature Al–Si–Cu–Mg alloy via Mo addition. *Mater. Sci. Eng. A* **2015**, *620*, 181–189. [CrossRef]
11. De Luca, A.; Seidman, D.N.; Dunand, D.C. Mn and Mo additions to a dilute Al–Zr–Sc–Er–Si-based alloy to improve creep resistance through solid-solution- and precipitation-strengthening. *Acta Mater.* **2020**, *194*, 60–67. [CrossRef]
12. Farkoosh, A.R.; Dunand, D.C.; Seidman, D.N. Tungsten solubility in L12-ordered Al_3Er and Al_3Zr nanoprecipitates formed by aging in an aluminum matrix. *J. Alloys Compd.* **2019**, *820*, 153383. [CrossRef]
13. Zhang, J.-Y.; Gao, Y.-H.; Yang, C.; Zhang, P.; Kuang, J.; Liu, G.; Sun, J. Microalloying Al alloys with Sc: A review. *Rare Met.* **2020**, *39*, 636–650. [CrossRef]
14. Vlach, M.; Čížek, J.; Smola, B.; Melikhova, O.; Vlček, M.; Kodetová, V.; Hruška, P. Heat treatment and age hardening of Al–Si–Mg–Mn commercial alloy with addition of Sc and Zr. *Mater. Charact.* **2017**, *129*, 1–8. [CrossRef]
15. Sims, Z.C.; Rios, O.R.; Weiss, D.; Turchi, P.E.A.; Perron, A.; Lee, J.R.I.; Li, T.T.; Hammons, J.A.; Bagge-Hansen, M.; Willey, T.M.; et al. High performance aluminum–cerium alloys for high-temperature applications. *Mater. Horiz.* **2017**, *4*, 1070–1078. [CrossRef]
16. Czerwinski, F.; Shalchi Amirkhiz, B. On the Al–$Al11Ce_3$ eutectic transformation in aluminum–cerium binary Alloys. *Materials* **2020**, *13*, 4549. [CrossRef]
17. Zheng, Y.H.; Wang, Z.D.; Zhang, S.M. Microstructure of diphase dendrite in Al–35%La alloy during solidification. *J. Cryst. Growth* **2013**, *362*, 33–37. [CrossRef]
18. Zheng, Y.; Wang, Z. A novel periodic dendrite microstructure in Al–La binary alloy. *J. Cryst. Growth* **2010**, *318*, 1013–1015. [CrossRef]
19. Zhang, X.; Wang, S. First-principles study of thermodynamic properties and solubility of aluminum-rare-earth intermetallics. *Comput. Mater. Sci.* **2014**, *90*, 56–60. [CrossRef]
20. Liu, T.; Ma, T.; Li, Y.; Ren, Y.; Liu, W. Stabilities, mechanical and thermodynamic properties of Al–RE intermetallics: A first-principles study. *J. Rare Earths* **2022**, *40*, 345–352. [CrossRef]
21. Togo, A.; Tanaka, I. First principles phonon calculations in materials science. *Scr. Mater.* **2015**, *108*, 1–5. [CrossRef]
22. Mao, Z.; Chen, W.; Seidman, D.; Wolverton, C. First-principles study of the nucleation and stability of ordered precipitates in ternary Al–Sc–Li alloys. *Acta Mater.* **2011**, *59*, 3012–3023. [CrossRef]
23. Mao, Z.; Seidman, D.N.; Wolverton, C.J.A.M. First-principles phase stability, magnetic properties and solubility in aluminum–rare-earth (Al–RE) alloys and compounds. *Acta Mater.* **2011**, *59*, 3659–3666. [CrossRef]
24. Sun, S.; Li, X.; Wang, H.; Jiang, H.; Lei, W.; Jiang, Y.; Yi, D. First-principles investigations on the electronic properties and stabilities of low-index surfaces of L12–Al3Sc intermetallic. *Appl. Surf. Sci.* **2013**, *288*, 609–618. [CrossRef]

25. Li, R.Y.; Duan, Y.H. Electronic structures and thermodynamic properties of $HfAl_3$ in $L1_2$, $D0_{22}$ and $D0_{23}$ structures. *Trans. Nonferrous Met. Soc. China* **2016**, *26*, 2404–2412. [CrossRef]
26. Sholl, D.S.; Steckel, J.A. *Density Functional Theory: A Practical Introduction*; John Wiley Sons: Hoboken, NJ, USA, 2022.
27. Hafner, J. Ab-initio simulations of materials using VASP: Density-functional theory and beyond. *J. Comput. Chem.* **2008**, *29*, 2044–2078. [CrossRef]
28. Blöchl, P.E.; Jepsen, O.; Andersen, O.K. Improved tetrahedron method for Brillouin-zone integrations. *Phys. Rev. B* **1994**, *49*, 16223–16233. [CrossRef]
29. Kresse, G.; Joubert, D. From ultrasoft pseudopotentials to the projector augmented-wave method. *Phys. Rev. B* **1999**, *59*, 1758–1775. [CrossRef]
30. Lee, C.; Yang, W.; Parr, R.G. Development of the Colle-Salvetti correlation-energy formula into a functional of the electron density. *Phys. Rev. B* **1988**, *37*, 785–789. [CrossRef]
31. Monkhorst, H.J.; Pack, J.D. Special points for Brillouin-zone integrations. *Phys. Rev. B* **1976**, *13*, 5188. [CrossRef]
32. Feynman, R.P. Forces in molecules. *Phys. Rev.* **1939**, *56*, 340. [CrossRef]
33. Wang, V.; Xu, N.; Liu, J.-C.; Tang, G.; Geng, W.-T. VASPKIT: A user-friendly interface facilitating high-throughput computing and analysis using VASP code. *Comput. Phys. Commun.* **2021**, *267*, 108033. [CrossRef]
34. Moruzzi, V.L.; Janak, J.F.; Schwarz, K. Calculated thermal properties of metals. *Phys. Rev. B* **1988**, *37*, 790–799. [CrossRef] [PubMed]
35. Debye, P. The theory of specific warmth. *Ann. Der Phys.* **1912**, *39*, 789–839. [CrossRef]
36. Otero-De-La-Roza, A.; Abbasi-Pérez, D.; Luaña, V. Gibbs2: A new version of the quasiharmonic model code. II. Models for solid-state thermodynamics, features and implementation. *Comput. Phys. Commun.* **2011**, *182*, 2232–2248. [CrossRef]
37. Han, F.; Yuan, M.; Wei, Z.; Yao, Y.; Yao, L.; Xin, L.; Shen, X. First-principles study of the Ti/Al3Ti interfacial properties. *Appl. Surf. Sci.* **2021**, *544*, 148960. [CrossRef]
38. Lu, C.; Ping, P.; Guifa, L.; Jinshui, L.; Shaochang, H. First-principle calculation of point defective structures of B2-RuAl intermetallic compound. *Rare Met. Mater. Eng.* **2006**, *35*, 1065–1070.
39. Ma, L.; Wang, Z.P.; Huang, G.H.; Huang, J.L.; Tang, P.Y.; Fan, T.W. Magnetic Phase Transition, Elastic and Thermodynamic Properties of $L1_2$-$(Ni, Cu)_3$ (Al, Fe, Cr) in 3 *d* High-Entropy Alloys. *Crystals* **2020**, *10*, 1102. [CrossRef]
40. Ravindran, P.; Fast, L.; Korzhavyi, P.A.; Johansson, B.; Wills, J.; Eriksson, O. Density functional theory for calculation of elastic properties of orthorhombic crystals: Application to TiSi2. *J. Appl. Phys.* **1998**, *84*, 4891–4904. [CrossRef]
41. Mattesini, M.; Ahuja, R.; Johansson, B. Cubic Hf_3N_4 and Zr_3N_4: A class of hard materials. *Phys. Rev. B* **2003**, *68*, 184108. [CrossRef]
42. Hill, R. The Elastic Behaviour of a Crystalline Aggregate. *Proc. Phys. Soc. Sect. A* **1952**, *65*, 349. [CrossRef]
43. Wu, Z.J.; Zhao, E.J.; Xiang, H.P.; Hao, X.F.; Liu, X.J.; Meng, J. Crystal structures and elastic properties of superhard Ir N_2 and Ir N_3 from first principles. *Phys. Rev. B* **2007**, *76*, 054115. [CrossRef]
44. Mouhat, F.; Coudert, F.-X. Necessary and sufficient elastic stability conditions in various crystal systems. *Phys. Rev. B* **2014**, *90*, 224104. [CrossRef]
45. Pugh, S.F. XCII. Relations between the elastic moduli and the plastic properties of polycrystalline pure metals. *Lond. Edinb. Dublin Philos. Mag. J. Sci.* **1954**, *45*, 823–843. [CrossRef]
46. Liu, T.; Ren, Y.; Li, Y. First-principles calculation on structure stability, thermodynamic and mechanical properties of Mg_2Si intermetallics. *Sci. Sin. Phys. Mech. Astron.* **2016**, *46*, 084611. [CrossRef]
47. Perdew, J.P.; Burke, K.; Wang, Y. Generalized gradient approximation for the exchange-correlation hole of a many-electron system. *Phys. Rev. B* **1996**, *54*, 16533–16539. [CrossRef]
48. Chen, X.R.; Zeng, Z.Y.; Liu, Z.L.; Cai, L.C.; Jing, F.Q. Elastic anisotropy of ϵ-Fe under conditions at the Earth's inner core. *Phys. Rev. B* **2011**, *83*, 132102. [CrossRef]
49. Deng, L.; Liu, X.; Liu, H.; Dong, J. High-pressure phase relations in the composition of albite $NaAlSi_3O_8$ constrained by an ab initio and quasi-harmonic Debye model, and their implications. *Earth Planet. Sci. Lett.* **2010**, *298*, 427–433. [CrossRef]
50. Errandonea, D.; Kumar, R.S.; Gracia, L.; Beltran, A.; Achary, S.N.; Tyagi, A.K. Experimental and theoretical investigation of ThGeO 4 at high pressure. *Phys. Rev. B* **2009**, *80*, 094101. [CrossRef]
51. Fu, H.; Zhao, Z.; Liu, W.; Peng, F.; Gao, T.; Cheng, X. Ab initio calculations of elastic constants and thermodynamic properties of γTiAl under high pressures. *Intermetallics* **2010**, *18*, 761–766. [CrossRef]
52. Khenioui, Y.; Boulechfar, R.; Maazi, N.; Ghemid, S. FP-LAPW investigation of Al_3 (Sc_{1-x} Ti_x) alloys properties in $L1_2$ and $D0_{22}$ structures. *Int. J. Mod. Phys. B* **2018**, *32*, 1850167. [CrossRef]
53. Tao, X.; Ouyang, Y.; Liu, H.; Zeng, F.; Feng, Y.; Jin, Z. Calculation of the thermodynamic properties of b2 AlRE (RE = sc, y, la, ce–lu). *Phys. B: Condens. Matter* **2007**, *399*, 27–32. [CrossRef]
54. Powell, B.R.; Rezhets, V.; Balogh, M.P.; Waldo, R.A. Microstructure and creep behavior in AE42 magnesium die-casting alloy. *Jom* **2002**, *54*, 34–38. [CrossRef]
55. Zhang, J.; Yu, P.; Liu, K.; Fang, D.; Tang, D.; Meng, J. Effect of substituting cerium-rich mischmetal with lanthanum on microstructure and mechanical properties of die-cast Mg–Al–RE alloys. *Mater. Des.* **2009**, *30*, 2372–2378. [CrossRef]

56. Zhang, J.; Liu, K.; Fang, D.; Qiu, X.; Tang, D.; Meng, J. Microstructure, tensile properties, and creep behavior of high-pressure die-cast $Mg_{-4}Al_{-4}RE_{-0.4}$ Mn (RE= La, Ce) alloys. *J. Mater. Sci.* **2009**, *44*, 2046–2054. [CrossRef]
57. Chen, Y.; Hammerschmidt, T.; Pettifor, D.; Shang, J.-X.; Zhang, Y. Influence of vibrational entropy on structural stability of Nb–Si and Mo–Si systems at elevated temperatures. *Acta Mater.* **2009**, *57*, 2657–2664. [CrossRef]

Disclaimer/Publisher's Note: The statements, opinions and data contained in all publications are solely those of the individual author(s) and contributor(s) and not of MDPI and/or the editor(s). MDPI and/or the editor(s) disclaim responsibility for any injury to people or property resulting from any ideas, methods, instructions or products referred to in the content.